REVIEW

Review of Design and Control Optimization of Axial Flux PMSM in Renewable-energy Applications

Jianfei Zhao, Xiaoying Liu, Shuang Wang* and Lixiao Zheng

Abstract

Axial flux permanent magnet synchronous motors (AFPMSMs) have been widely used in wind-power generation, electric vehicles, aircraft, and other renewable-energy applications owing to their high power density, operating efficiency, and integrability. To facilitate comprehensive research on AFPMSM, this article reviews the developments in the research on the design and control optimization of AFPMSMs. First, the basic topologies of AFPMSMs are introduced and classified. Second, the key points of the design optimization of core and coreless AFPMSMs are summarized from the aspects of parameter design, structure design, and material optimization. Third, because efficiency improvement is an issue that needs to be addressed when AFPMSMs are applied to electric or other vehicles, the development status of efficiency-optimization control strategies is reviewed. Moreover, control strategies proposed to suppress torque ripple caused by the small inductance of disc coreless permanent magnet synchronous motors (DCPMSMs) are summarized. An overview of the rotor-synchronization control strategies for disc contra-rotating permanent magnet synchronous motors (CRPMSMs) is presented. Finally, the current difficulties and development trends revealed in this review are discussed.

Keywords AFPMSM, Design optimization, Cogging torque, Efficiency optimization, Control strategy optimization

1 Introduction

The permanent magnet disc machine developed in the 1970s attracted considerable research attention in the 1980s. Campbell proposed an axial-field DC machine with a disc-shaped armature [1, 2]. The parameters of this novel motor topology were calculated using a computer program [3], and subsequently, permanent magnet disc motors were investigated. Moreover, permanent magnet synchronous motors (PMSMs) have been widely used owing to their high power density and reliability [4]. Thus, research on axial flux permanent magnet synchronous motors (AFPMSMs) has attracted attention.

Compared with radial-flux permanent magnet synchronous motors (RFPMSM), AFPMSMs have many advantages. First, the effective part of an AFPMSM is the area perpendicular to its axis, and the wire cuts the magnetic induction line in the radial direction, resulting in stator and rotor-disc structures. The disc structure can be smaller and more compact under the same performance requirements. Therefore, AFPMSMs have wider applications in electric vehicles, wind-power generation, and marine propulsion, where the motor size and efficiency requirements are high. An AFPMSM has a flat structure with short axial dimensions and is suitable in cases of limited axial space, particularly in the wheels of electric vehicles. In Ref. [5], a brushless AFPMSM design method focusing on electric traction was proposed, and the installation-position option was provided. Various installation methods can be selected according to the size of the body space and required power. Second, owing to

*Correspondence:
Shuang Wang
wang-shuang@shu.edu.cn
School of Mechatronic Engineering and Automation, Shanghai University, Shanghai 200444, China

the symmetrical arrangement of the AFPMSM stators and rotors, the stator windings have good heat-dissipation conditions, and they can be designed with higher power densities. In Ref. [6], an AFPMSM was designed for low-speed wind turbines where the two rotor discs with a central stator function naturally acted as fans. Thus, the heat and iron losses caused by the copper coil were eliminated. The disc-shaped stator and rotor of an AFPMSM are arranged in an identical manner to ensure their facile modularization and superposition. The number of phases can be increased by increasing the number of stacks. Multiphase machines are commonly used in marine applications. In Ref. [7], a ring-winding AFPMSM used in a rim-driven thruster for ship electric propulsion was designed. Because the motor and propeller were integrated in a single unit, this ring-winding AFPMSM exhibited high reliability and a simple structure, and the number of poles and phases therein could be easily increased. Additionally, AFPMSMs have large torque-to-mass ratios, run smoothly at low speeds, and exhibit good dynamic performance [8–10].

AFPMSMs have been comprehensively reviewed in this paper. In Section 2, the topologies of AFPMSMs are introduced and classified according to the number of stators and rotors, core material, presence or absence of stator slots, winding shape, and placement of the permanent magnet.

In Section 3, the methods for designing AFPMSMs with an iron core to optimize motor parameter design, structure design, and material are summarized. Section 4 summarizes the research on the disc coreless permanent magnet synchronous motor (DCPMSM) design-optimization methods, where motor-structure design-optimization methods are introduced separately for the rotor and stator.

Section 5 provides a detailed overview of the research status on and trends in cogging-torque minimization methods, which are common optimization issues in motor design. For an AFPMSM, motor-design optimization is mainly used to suppress cogging torque. Therefore, the application of various design methods such as magnet skew, displacement, and pole-arc optimization are reviewed, and the cogging-torque model establishment and parameter optimization methods are summarized.

The control strategy optimization for AFPMSMs is summarized in Section 6 in three parts: status of the research on efficiency-optimization strategies, torque-ripple minimization control strategies for DCPMSMs, and rotor-synchronization control strategies for contra-rotating permanent magnet synchronous motors (CRPMSMs). First, owing to the prevalence of AFPMSMs in electric vehicles and other applications, efficiency optimization is an indispensable for the design and control

of AFPMSMs. Further improvements in the efficiency of motor are difficult, and some studies have taken advantage of the coordinated operation of AFPMSM stators and rotors to propose an efficiency optimization control strategy. At present, the main efficiency-optimization control strategies are torque distribution and winding switching. Next, because of the electromagnetic torque-ripple problem caused by the small stator inductance in DCPMSMs, a control strategy proposed to solve this problem is summarized. Third, to address the rotor out-of-step problem of the CRPMSM when the torque is unbalanced, a rotor synchronization control strategy is summarized.

Finally, the difficulties currently associated with the research on AFPMSMs and future development prospects therein are summarized.

A summary layout diagram of this paper is shown in Figure 1.

2 Topology and Classification of AFPMSMs

The classification of AFPMSM topologies can be represented using six-levels [11], as shown in Table 1.

The first level categorizes AFPMSMs into four types according to the number of stators and rotors [12, 13]: single-stator single-rotor (SSSR), axial-flux internal rotor (AFIR), toroidal stator (torus), and multi disc [14]; this level was adopted to introduce AFPMSMs in this review.

In the second level, the stator structures are categorized as iron core and coreless.

In the third level, AFPMSMs with an iron core are categorized as slotted and slotless stators [13, 15].

In the fourth level, torus motors are classified based on magnetic polarity at the corresponding positions on the two rotors. Therefore, the two types of torus motors are parallel (NN) and series (NS) magnetic circuit structures.

In the fifth level, AFPMSMs are classified based on two stator-winding structures. A winding structure called "drum winding" surrounds the stator in the radial and circumferential directions, as shown in Figure 2(a). Drum windings can be either non-overlapping or overlapping [16]. These coils are evenly distributed along the diameter of the stator core in the opposite position such that each phase has an equal number of oppositely connected coils to eliminate the magnetic flux circulation that may occur in the stator core [17]. Toroidal windings surround the stator in the radial and axial directions and are always non-overlapping, as shown in Figure 2(b). Non-overlapping windings simplify the winding assembly but affect the output torque to a certain extent owing to their small winding factor [16]. When toroidal windings are used in torus motors, as shown in Figure 3, radial windings are used to generate torque to maximize the active portions of the windings, resulting in relatively short
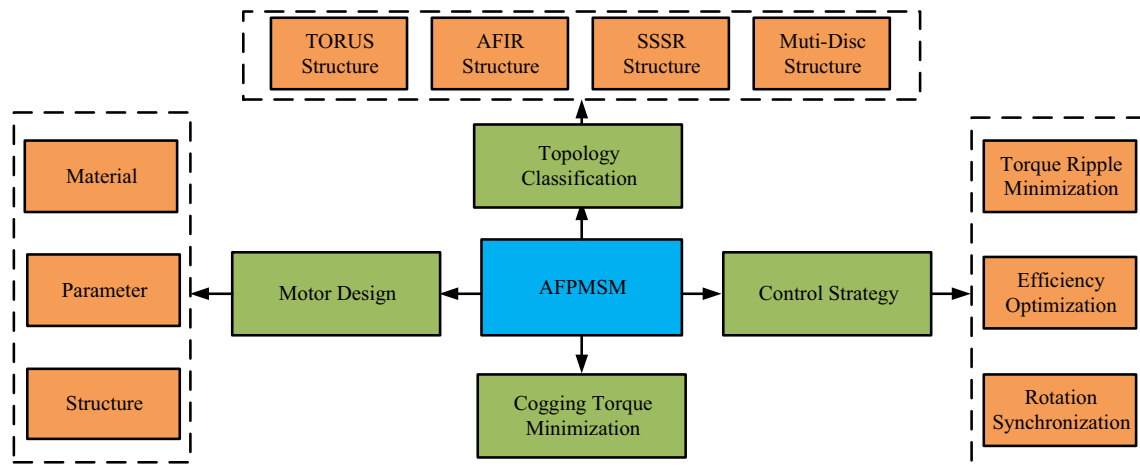
Zhao *et al. Chinese Journal of Mechanical Engineering*   (2023) 36:45

Page 3 of 21

Figure 1 Organization of the paper

Table 1 Classification of AFPMSMs

AFPMSM								
Structure	SSSR		AFIR		Torus				Multi-disc
Core	Iron core		Iron core		Iron core			Coreless	
Slotting	Slotted	Slotless	Slotted (AFIR-S)	Slotless (AFIR-NS)	Slotted (Torus-S)			Slotless (Torus-NS)	
Magnetic circuit	NS		NS(NN)		NN		NS	NN	NS
Winding	Drum	Toroidal	Drum	Toroidal	Drum	Toroidal	Drum	Toroidal	Drum
Special structure					CRPMSM-TORUS-NS YASA AFPMSM-TORUS				

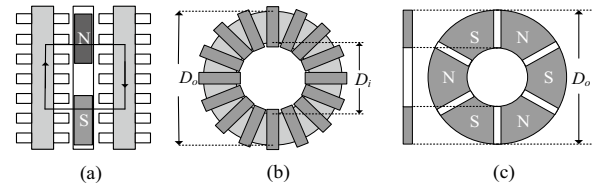**Figure 2** Winding structure of AFPMSM: **a** Drum and **b** Toroidal windings

Figure 4 Sectional view of an AFIR-NS motor: **a** Magnetic circuit, **b** Stator structure, and **c** Rotor structure
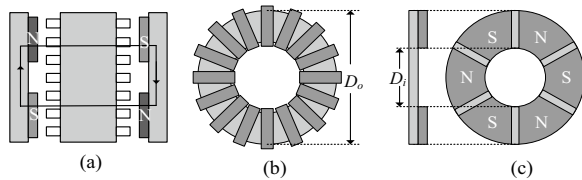

Figure 3 Sectional view of a torus-NS motor: **a** Magnetic circuit, **b** Stator structure, and **c** Rotor structure

end windings. Short end windings provide lower copper losses and higher efficiencies [18]. As shown in Figure 4, when toroidal windings are used for AFIR motors, part of the windings is used to generate torque and is located on the inner side of the stator facing the rotor. As a result, the end windings in the AFIR-NS topology are relatively long, resulting in a lower efficiencies and higher copper losses.

At the sixth level, two types of CRPMSMs with special structures are introduced, which are deformed by changing the winding structure of the torus-NS motor. A yokeless and segmented armature (YASA) AFPMSM is a torus motor without a stator yoke.

The heat dissipation and increase in temperature depending on the motor structural characteristics of AFPMSMs are also investigated. The electromagnetic and thermal design of a motor directly determines its

service life, efficiency, and manufacturing cost [19, 20]. To determine the increase in the temperature of a motor, a thermal analysis model must be established for AFPMSMs that not only monitors whether the clicks are in a normal running state but also provides guidance for the parameter configuration of the motor design. In Ref. [21], a lumped-circuit thermal-analysis model for an AFPMSM was established. The increase in temperature determined from the thermal analysis provided guidance for the configuration of the frequency, current density, and air-gap flux-density values and selection of materials. In Ref. [22], the thermal and demagnetization analyses of an AFPMSM for railway vehicle propulsion are discussed. The motor components were tested under three working conditions to obtain temperature images. The motor temperature was monitored to determine whether the permanent magnet became demagnetized owing to overheating during normal operation. In Ref. [23], based on the structural characteristics of an AFPMSM, convective cooling was reported to have a significant impact on the thermal design of a motor. Therefore, an electromagnetic and thermal coupling model was introduced and verified by comparing the model results with actual thermal-image measurement results.

Compared with a traditional radial PMSM, the stator windings of an AFPMSM provide better heat dissipation in terms of structure, and they can be designed with higher power densities. Additionally, to obtain better heat dissipation and enhance the cooling effect, the structure of an AFPMSM can be optimized via water-and oil-cooling methods. In Ref. [24], the heat-dissipation capacity was increased by optimizing the stator structure and using the water-cooling method; furthermore, three structures were designed and compared using a thermal analysis. In Ref. [25], the structure of a motor end winding was improved using the water-cooling method to enhance heat dissipation. In Ref. [26], a motor end winding was directly oil-cooled, and the performance of the machine was compared with that after water-cooling.

2.1 SSSR Motor

The SSSR motor structure is the most elementary structure, which is composed of a stator consisting of a winding, an iron disc, and a rotor manufactured from a steel disc [18]. Owing to the presence of only one air gap, the large axial force exerted on the stator by the rotor can easily damage the motor structure if the mechanical design or assembly is ineffective. Moreover, the magnetic field of the rotor alternates in the stator and causes losses, thereby reducing the operating efficiency of the motor. Therefore, SSSR motors are not widely used in practical situations.
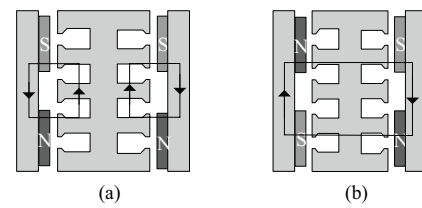

Figure 5 Magnetic circuit type of a torus-S motor: **a** NN and **b** NS type
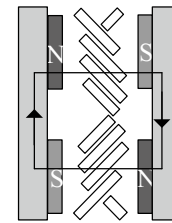

Figure 6 Magnetic circuit of a coreless torus-NS motor

2.2 Torus Motor

A single-stator–dual-rotor AFPMSM is a PMSM with a toroidal stator (torus) structure [11, 18]. The stator of the torus motor is sandwiched between two permanent-magnet rotors, which consist of steel discs with NdFeB permanent magnets and a shaft, as shown in Figure 3(c). Torus motors are either slot (torus-S) or slotless (torus-NS). The torus-NS motor demonstrates better performance owing to its simple stator production, small motor leakage inductance, and small torque fluctuations; however, it uses more permanent magnets, which increases the production cost.

Torus-S motors can be further classified as NN- and NS-types according to the form of the magnetic circuit [27, 28]. As shown in Figure 5(a), homopolar magnetic poles are located on the two rotors of the NN-type torus-S motor. The N and S magnetic poles on each side of the rotors form a parallel magnetic circuit with the air-gap, windings, and part of the stator core on this side. The two parallel magnetic circuits pass through the stator core in the circumferential direction and do not interfere with each other when the stator core is sufficiently thick.

As shown in Figure 5(b), heteropolar magnetic poles are located on the two rotors of the NS-type torus-S motor. The N and S magnetic poles on each side of the rotors form a series magnetic circuit with the air gap and windings on this side, which directly penetrates the stator core axially. The NS-type torus motor is a DCPMSM, as shown in Figure 6, and characterized by a small motor iron loss, small motor reactance, large current ripple, and difficult motor control. Figure 7 shows the magnetic circuit diagram of a torus-NS motor.
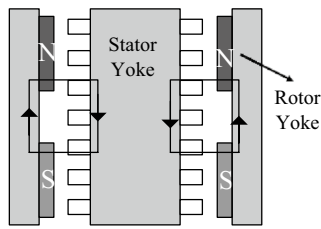
Zhao *et al. Chinese Journal of Mechanical Engineering*   (2023) 36:45

Page 5 of 21

Figure 7 Magnetic circuit of an NN-type torus-NS motor
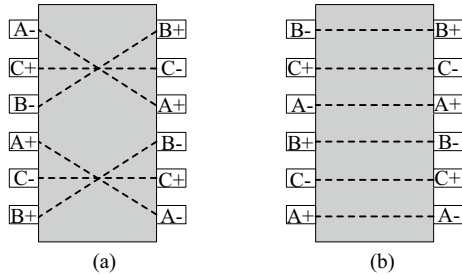
Figure 8 Winding types for an AFPMSM: **a** CRPMSM and **b** torus-NS PMSM

Figure 9 3-D winding structure of a CRPMSM

Figure 10 Magnetic circuits of an AFIR motor: **a** AFIR-NS and **b** AFIR-S

The CRPMSM is a special structure of the torus-NS motor, which is used to drive a counter-rotating propeller [29]. The CRPMSM was first proposed by Professor F. Caricchi of the University of Rome. It outputs mechanical energy by nesting the output shafts of two independent permanent magnet rotors, and the two shafts drive two propellers [30]. The structure of a CRPMSM is similar to that of a torus-NS motor; however, their winding structures are different. In Figure 8(a), the ends of the windings shown by the dashed lines indicate that the A- and B- phase windings of the stator are cross-wound on the core; thus, the phase sequences of the windings on the two sides of the stator core are opposite. When a three-phase alternating current is applied, a pair of magnetic fields rotating in opposite directions is generated on both sides of the stator. Figure 9 shows the winding structure of the CRPMSM [29], and Figure 8(b) shows the winding structure of the torus-NS motor. The opposite windings on the two sides of the stator core are connected at the ends of the windings, as shown by the dashed lines, to form various toroidal windings. The only difference between Figure 8(a) and (b) is that the magnetic fields on the two sides of the stator core rotate in the same direction in the winding structure shown in the latter [31].

2.3 AFIR Motor

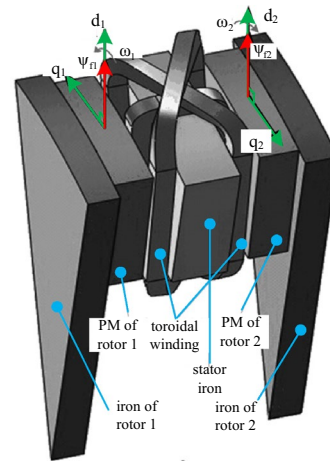A dual-stator–single-rotor AFPMSM exhibits an AFIR structure and consists of an intermediate rotor and two stators fixed on both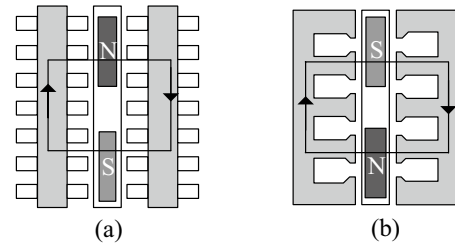 sides of the rotor. Both stators of the AFIR motor form a rotating magnetic field. Therefore, its control is more flexible, and it has a wider high-efficiency coverage. Therefore, a continuous, stable, and high-efficiency control strategy for AFIR motors must be investigated [32]. The rotor of the AFIR motor is composed of axially magnetized NdFeB permanent magnets and a shaft without a steel disc that is slightly different from that of a torus motor. To form a rigid structure to hold the magnets without a rotor disc, non-magnetic materials are used to fill the space between the magnets [18], as shown in Figure 4(c). Thus, an AFIR motor exhibits a power-to-inertia ratio higher than that of a torus motor. AFIR motors can be slotted (AFIR-S) or slotless (AFIR-NS). Figure 10(a) and (b) show the magnetic circuits of AFIR-NS and AFIR-S motors, respectively. Figure 11 shows the structure of an AFIR-S motor [30]. In general, no steel disc exists in the rotor of the AFIR motor, whose magnetic circuit type is NS. However, to make control more convenient, some studies have divided the steel disc of the rotor into two isolated parts and placed permanent magnets facing the stators on both sides to form an NN-type magnetic circuit, as shown in Figure 12 [33, 34].
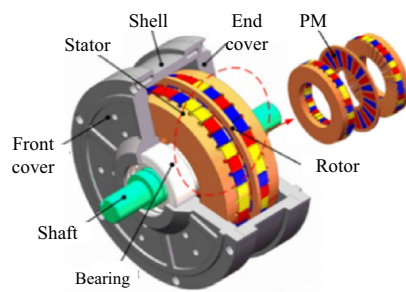
Zhao *et al. Chinese Journal of Mechanical Engineering* (2023) 36:45

Page 6 of 21
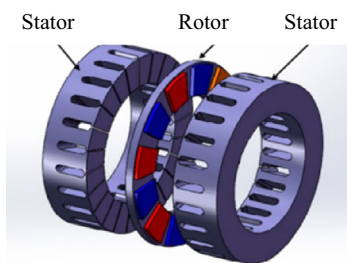

Figure 11 Structure of AFIR-S motor

Figure 12 Structure of an NN-type AFIR-S motor

2.4 Multi-Disc Motor

A multi-disc motor consists of several stacked AFIR- and torus-structure motors. Generally, an SSSR motor increases the motor torque by increasing the disc diameter. However, owing to the limitations of the axial force exerted by bearings and the disc stiffness, the extent to which the torque can be increased is limited. Therefore, a multi-disc motor is a better solution for high-torque transmission devices [17]. Additionally, because the power of an AFPMSM is independent of its axial length, the number of stators can be increased to improve the output power of the motor [35].

Sections 2.1, 2.2, 2.3 and 2.4 described the advantages and disadvantages of various AFPMSM structures based on the number of stators and rotors. An overview is provided in Table 2.

3 Design and Optimization of an AFPMSM with an Iron Core

Motor-design methods have been extensively investigated. The key aspect of motor design is electromagnetic performance design. The most commonly used methods include the size equation [11, 31, 36, 37], finite element analysis (FEA) [31, 38, 39], equivalent magnetic circuit [40, 41], and analytical calculation methods [42, 43]. The improvements in motor-design methods are essential for motor optimization, and many studies have focused on broader prospects of optimization. This article reviews the optimization methods for motor parameters, structure design, and materials [44].

3.1 Parameter Optimization

Because of the strong coupling and nonlinear relationship between the various motor parameters, some studies have transformed the optimization of motor design into a multi-objective optimization problem, i.e., adopted an improved parameter-optimization method to design motor parameters more accurately.

Cvetkovski et al. aimed to minimize the rotor mass of a dual-stator–single-rotor motor using a genetic algorithm to optimize the parameter calculation [45]. As a result, the motor mass was reduced from 24.096 to 20.016 kg to achieve a lightweight motor design. The effectiveness of the genetic algorithm was verified by comparing the air-gap flux-density distribution and magnetic field under no-load and rated-load conditions. Luo et al. used a hybrid optimization algorithm, which incorporated the response-surface method, variable-density method, and particle-swarm optimization (PSO) algorithm, to optimize the size and topology of an in-wheel AFPMSM to reduce the motor mass [46].

A surrogate-assisted multi-objective optimization algorithm (SAMOO) was proposed to replace 3-D FEM analysis [47]. The SAMOO achieved an evenly distributed and accurate Pareto front set without requiring a large number of functions. To verify the superiority of SAMOO over traditional multi-objective optimization algorithms, the skew and pole-arc to pole-pitch ratio of a torus motor were optimized. As a result, the motor torque amplitude increased from 1.39 to 1.45 Nm, and the torque ripple decreased from 79.35% to 7.24%. Akinci

Table 2 Advantages and disadvantages of various AFPMSM structures

Structure		Advantages	Disadvantages
SSSR		Simple structure, good heat dissipation	Large axial magnetic pull, low efficiency, Easy to damage
Torus	Torus-NS	Low torque ripple	High production cost
	Torus-S	Small iron loss	Large current ripple, difficult to control
AFIR		Small moment of inertia, High torque density	Large hysteresis loss, Large eddy current loss
Multi-disc		High output power, high power density	Large space occupancy

Zhao et al. Chinese Journal of Mechanical Engineering   (2023) 36:45
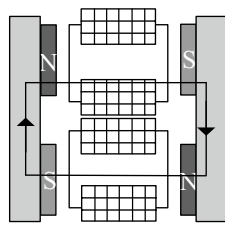
Page 7 of 21

Figure 13 Topology of the YASA structure of an AFPMSM

and Polat adopted a genetic algorithm to optimize a motor design to maximize motor efficiency [48].

3.2 Structural Optimization

Developing a new motor structure is important for the optimization of motor performance, and one of the main optimization goals is lightweight motors. Woolmer et al. proposed a YASA structure for an AFPMSM. Based on the traditional torus motor, the entire stator was replaced with segmented stators fixed on the casing, and the stator yoke was removed. Furthermore, as shown in Figure 13, square coils were used to efficiently utilize the slot space to achieve a high fill factor, shorten the axial length of the motor, and further reduce the weight [49]. Consequently, the YASA motor had approximately 50% less stator weight, exhibited a 20% increase in torque density, and reached 95% efficiency. A Korean study applied a stator coreless structure to a torus motor, which significantly reduced the motor weight [42]. A proposed single-phase flux-switching permanent magnet motor (FSPM) with a tapered rotor pole resulted in different air-gap reluctances along the path from one side of the rotor pole to the other, thereby enhancing the capability of unidirectional rotation and improving the self-starting torque [50]. Furthermore, a new axial ferrite-magnet-assisted synchronous reluctance motor was reported to use less magnetic material to achieve a higher torque density [51].

3.3 Material Optimization

The most important goals of motor-design optimization are lightweight and performance enhancement. With the development of new materials, material optimization has become an important aspect in motor-design optimization, and alternative materials have been developed for each motor part. The magnetic material is an important component, and its weight and performance have a significant influence on the power density and operational efficiency of a motor. Soft-magnetic materials are the primary materials used in motors. They are ideal substitutes for steel cores because of their low eddy-current and hysteresis losses and are widely used nowadays [39, 52]. The most commonly used soft magnetic materials are

soft-magnetic alloys, soft-magnetic composites (SMCs), and amorphous metals (AMMs).

Ni-Fe and Co-Fe are the most common soft-magnetic alloys. Ni–Fe produces a lower core loss than Co–Fe and is more in line with the requirements of high-speed low-torque motors, while Co–Fe is more suitable for low-speed high-torque motors because it achieves higher flux densities. Therefore, the use of soft-magnetic alloys largely depends on the performance requirements of the motors [53–55]. SMCs are the most widely used materials for motor design. The SMC core is usually manufactured by bonding or sintering iron particles with a polymer or resin or by pressing the iron particles. Various studies have proven that SMCs are a good choice for high-speed motors because of their low flux densities [53], resistivities better than those of AMMs, and lower eddy-current losses. However, low permeability, low mechanical strength, weak anti-vibration ability, short service life, and degradation properties are factors that limit a wider use of SMCs [53, 56, 57]. Compared with soft-magnetic alloys and SMCs, AMMs exhibit lower core losses, higher coercivities, and higher permeabilities; therefore, AMMs are suitable for high-speed and high-frequency motors. However, the high hardness values of AMMs necessitate the use of precise cutting technologies when used in motor structures [58].

In Ref. [57], the performance of AFPMSMs was compared with those of electrical-steel and SMC cores over a wide frequency range. SMCs exhibited temperature characteristics worse than those of a steel core but smaller torque fluctuations in the high-frequency region and higher operating efficiencies. In Ref. [59], a YASA AFPMSM with an SMC core was proposed with a shoe-width ratio (α_s) adjustable in a large range, as shown in Figure 14. The back EMF waveform was closest to a sinusoidal distribution at $\alpha_s = 0.8$. A comparison of the back EMFs of the motor for various shoe-width ratios is shown in Figure 15.

In addition to using soft-magnetic materials to replace steel cores, coreless motors employ non-ferromagnetic materials in the stator core to reduce the motor mass and increase the torque and magnetic field density. In Refs.
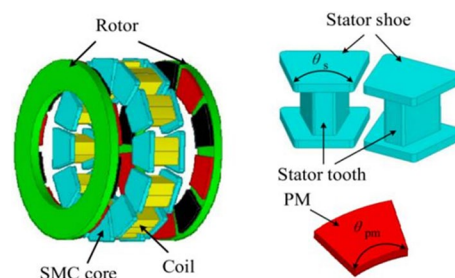

Figure 14 Structure of a YASA with an SMC core

Zhao *et al. Chinese Journal of Mechanical Engineering* (2023) 36:45
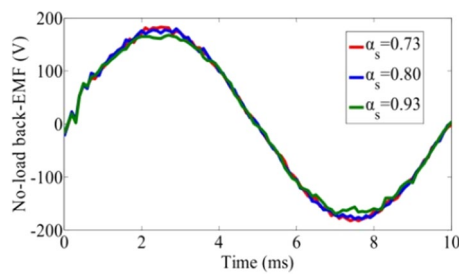
Page 8 of 21

Figure 15 Comparison of back EMFs for various shoe-width ratios

[52, 60], the feasibility of replacing the rotor and stator with non-ferromagnetic materials was comprehensively analyzed in terms of magnetic flux path, selection of alternate materials, manufacturing techniques, and production and cost advantages. Moreover, thermoplastics such as Polybenzimidazole (PBI), Polyamide imide (PAI), Polyphenylene sulfide (PPS), and Polyether ether ketone (PEEK) that satisfy the mechanical strength and thermal stability of a motor rotor have been introduced. Table 3 presents a comparison of the performance of thermoplastics with those of CE221 and 42CrMo4 steel, and suitable materials can be selected according to motor performance requirements.

4 Design and Optimization of an AFPMSM Without an Iron Core

Silicon-steel sheets with high permeability are usually laminated to form an iron core in AFPMSMs to increase their magnetic induction intensities by reducing their magnetic reluctance. However, an iron core increases the volume and weight of a motor, which restricts its applicability when the size of the motor is limited [61]. Owing to the slot effect, the electromagnetic torque ripple cannot be ignored when an iron-core motor is running. Meanwhile, the hysteresis and eddy-current losses caused by an iron core under the action of a rotating magnetic field account for more than 20% of the total motor loss and reduce motor efficiency. Therefore, NdFeB

permanent-magnetic materials with high coercive forces and remanence densities are applied to such motors to obtain sufficient magnetic potential to achieve the coreless motor structure shown in Figure 6. A DCPMSM has a compact axial structure, low mass, high power density, low vibration and noise, and high efficiency [62, 63]. As with AFPMSMs with cores, the design optimization of DCPMSM parameters, structures, and materials has been studied.

4.1 Parameter Design Optimization

Intelligent algorithms have been previously combined with traditional parameter-optimization methods for DCPMSMs to obtain the optimal parameter sets [64, 65]. In Ref. [64], to achieve maximum motor power density, a PSO algorithm was used to optimize the thickness of a permanent magnet, air-gap length, pole-arc coefficient, and thickness and inner radius of the winding disc, resulting in approximately 80% increase in the power density. Le et al. employed a support vector machine with an orthogonal design to establish an accurate model [66]. To obtain a global optimal solution between torque ripple and output torque, a genetic algorithm was added for the target optimization. Under the same working conditions, the output torque was increased by 18.5%, and the torque ripple was reduced by 33%. Aydin et al. used the size approach method to obtain the highest power density, least weight, and highest torque-to-weight ratio [67]. The number of motor poles was first determined to be 24, and the magnetic equivalent circuit was used for the magnetic modeling and the design of the initial parameters for several turns, magnetic pole-arc ratios, and other factors. Finally, a reliable coreless dual-rotor AFPMSM was designed for solar vehicles based on 3D-FEA. In Ref. [65], a new method was proposed to determine the axial component of the magnetic flux density and more accurately calculate the optimal thickness of a rotor disc, based on the deflection of the rotor, to reduce the motor mass.

Table 3 Properties of high-performance thermoplastics

Material	PEEK	PPS	PAI	PBI	CE221	42CrMo4 Steel
Tensile strength at 25 °C (MPa)	110	93	150	110	92	1000
Tensile strength at 65 °C (MPa)	82.7	55.2	150	110	n/a	1000
Flexural strength(MPa)	172	145	190	221	131	n/a
Thermal conductivity (W/(m·K))	0.252	0.288	0.260	0.403	0.167	40
Density (g/cm³)	1.31	1.35	1.41	1.3	1.21	7.8
Water absorption (%)	0.1	0.01	0.35	0.4	0.21	n/a
Heat deflection temperature (°C)	160	120	280	425	201	n/a

Zhao *et al. Chinese Journal of Mechanical Engineering* (2023) 36:45

Page 9 of 21

4.2 Structural Design Optimization

The structural design of a DCPMSM is mainly classified as rotor and stator structures.

4.2.1 Rotor Structure

Because of the lack of an iron core, a DCPMSM exhibits a low magnetic flux density; however, a PMSM requires an air-gap magnetic flux density with as large a fundamental wave amplitude as possible to increase motor output torque, reduce winding current and losses, and thereby increase motor power density [68]. Two methods are available to improve the air-gap magnetic flux density [69]: one is to choose rare-earth permanent magnetic materials with high remanence densities, and the other is to optimize the magnetic steel structure. However, owing to the high price of rare-earth permanent magnetic materials, their use must be restricted without reducing the performance of the motor to save costs [70]. Therefore, the common means of optimization is to change the shape and arrangement of the magnets. DCPMSMs can be categorized as surface-mounted, interior, and Halbach types according to their permanent-magnetic structure.

The magnet shape of a surface-mounted AFPMSM can be semicircular, trapezoidal, rectangular, or circular [71, 72]. Figure 16 illustrates these four types. A trapezoidal permanent magnet is always preferred in the absence of a special requirement for the cogging torque, as it exhibits its most uniform magnetic-field distribution. Circular and rectangular permanent magnets are fixed in type and have low design costs. A circular permanent magnet exhibits the best torque-output capability. Under identical experimental conditions, the total harmonic distortion (THD) of the low-order harmonics of a semicircular permanent magnet is smaller than that of a trapezoidal permanent magnet; however, the THD of the high-order harmonics of a semicircular permanent magnet is larger.

In terms of the interior structure, an AFPMSM with sinusoidal rotor segments (AF-IPM) was proposed [73], as shown in Figure 17. The torque density of the AF-IPM was 35.7% higher than that of a surface-mounted AFPMSM with the same stator, its fundamental wave of the back EMF was 16% higher, and the THD of its back EMF was 61.44% lower; however, it produced a slightly higher torque ripple.
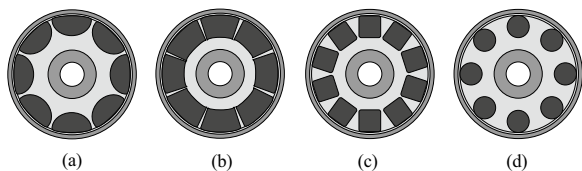

Figure 16 AFPMSM permanent-magnet shapes: **a** Semicircular, **b** Trapezoidal, **c** Rectangular, and **d** Circular
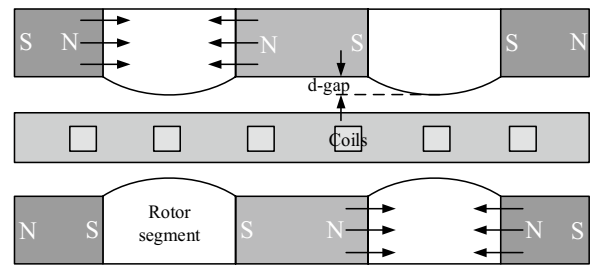

Figure 17 Structure of an AF-IPM

Gieras et al. first applied a Halbach array to a DCPMSM to obtain an air-gap flux density close to a sinusoid, thereby improving the motor power density and efficiency [74]. Figure 18 shows a sectional view of a dual-rotor DCPMSM based on a Halbach array. The Halbach array causes the magnetization vector to continuously rotate, which direction is as a function of the distance along the array. Thus, every two adjacent magnetization vectors are at an angle, and the commonly used angles are 90°,60°, and 45°, corresponding to two, three, and four blocks per pole [43]. Figure 19 shows the magnetization directions of permanent magnets at three different angles.

The torque ripple and back EMF of a motor are related to the sinusoidal characteristics of the air-gap flux density [75]. The Halbach array can improve the air-gap magnetic-field waveform. Therefore, a magnetic field that is closer to the sinusoidal distribution in space is obtained to reduce the cogging torque. Moreover, based on the superior ability of magnetic gathering, a Halbach array uses a combination of radial and tangential arrays to increase the magnetic field on one side and decrease the magnetic field on the other side to improve the air-gap flux density. In this case, the torque density of the motor increases, thereby reducing the size of the motor under the same torque capacity requirement. Compared with the conventional radial excitation motor, a motor based on a Halbach array has a lower no-load loss.

The performance of DCPMSMs has been previously improved using Halbach arrays. Wang et al. proposed a DCPMSM with a wedgy air-gap in which the slot space factors at the inner and outer diameters of the motor rotor were designed to have the same value, as shown in Figure 20 [75]. Static air-gap magnetic field analysis of the wedgy and even air gaps was carried out in this study. The wedgy air-gap DCPMSM exhibited significantly better performance indicators than those of the even air-gap DCPMSM. Specifically, its efficiency was 0.6% higher, and its air-gap density amplitude was 0.14 T higher.

The magnet structure of a DCPMSM based on a Halbach array can also be optimized. In Ref. [43], the edge
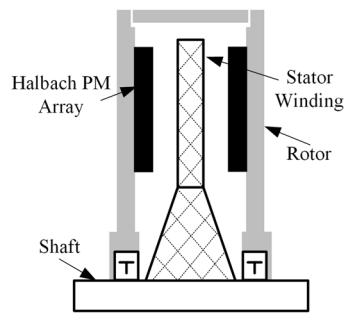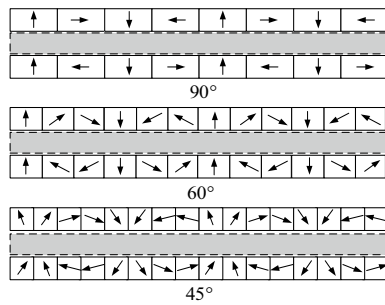
Figure 18 Sectional view of a DCPMSM
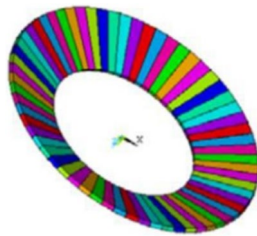

Figure 19 Halbach arrays

Figure 20 Structure of wedgy air-gap

Figure 21 Halbach arrays with various shapes of magnets: **a** Right angle, **b** Round, **c** Fillet, and **d** Rectangular chamfered

Figure 22 Winding structures: **a** Rhomboidal, **b** Circular, **c** Trapezoidal, and **d** Hybrid

4.2.2 Stator Structure

The optimization of a stator structure mainly involves changes to the stator windings. As mentioned in Section 1, stator windings can be drum or toroidal windings. Toroidal windings can only be non-overlapping, whereas drum windings can be overlapping or non-overlapping. Because non-overlapping windings can achieve performance similar to those of overlapping windings with less copper content, in some cases the torque performance is better [76]. This has resulted in more extensive research into the application of non-overlapping windings.

The most commonly used winding shapes include trapezoid, rhomboid, hexagon, and circular [72]. In Ref. [77], a hybrid winding with a better performance was proposed, as shown in Figure 22(d). This new type of winding combined the advantages of circular and trapezoidal windings with short ends and a small winding resistance. Therefore, the copper loss was lower, and the power density and back EMF was higher. Moreover, the superiority of the hybrid winding was verified by comparing the 3D-FEA of trapezoidal, rhomboidal, circular, and hybrid windings. Zhang et al. used single-layer concentrated windings on a single-stator–dual-rotor DCPMSM to reduce the air-gap length, thereby increasing the power density and verified the reliability of this method via 3D-FEA [78].

shape of the permanent magnet of a 90° Halbach array was optimized to an outer circle, inner circle, and rectangular chamfer, as shown in Figure 21. FEA was used to analyze the fundamental wave amplitude and sinusoidal characteristics of the air-gap magnetic field. The optimized permanent-magnet shape reduced the magnetic leakage between the permanent magnets and low-order harmonic content of the air-gap magnetic flux density, thus making the waveform closer to a sinusoid. Among these shapes, the inner circle proved to be optimal. Upon further investigation, the air-gap magnetic flux densities of the 90° and 45° arrays with optimized magnets were found to be the same; however, the installation and magnetization of the 90° array was more convenient.
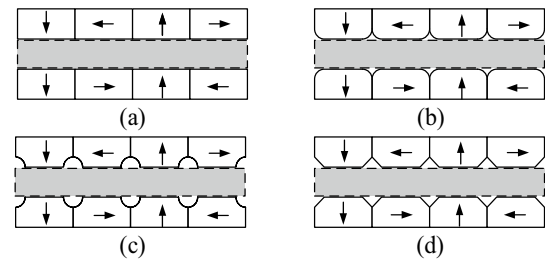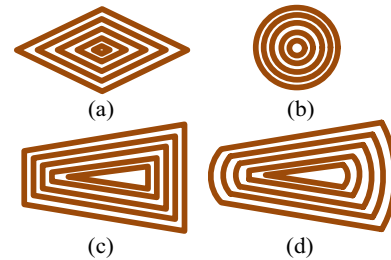
Zhao *et al. Chinese Journal of Mechanical Engineering*   (2023) 36:45

Page 11 of 21

Figure 23 Simulation model of AFPMSM with PCB stator

Figure 24 Structure of AFPMSM with hybrid PCB coil

Figure 25 Structure of miniature AFPMSM with rhomboidal PCB coil

Figure 26 3-D finite simulation model of a hexagon PCB coil
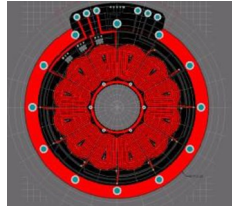
The manufacture level of a stator winding not only determines its life, heat resistance, and mechanical strength but also the smallest air gap that may be achieved using it. Two stator winding manufacturing methods exist for disc motors: wire winding and printing. Currently, wire winding is the most commonly used method and requires high-precision windings to ensure consistency; thus, the manufacturing process is complicated. With the development of printing technology, the maximum number of layers and thickness of copper achievable on printed circuit boards (PCBs) have increased, and the costs associated with them have decreased. This has attracted attention to PCB stators with good precision and consistency. Figure 23 shows the simulation model of a DCPMSM with a PCB stator. The optimization of the application of PCB stators in AFPMSMs has been extensively studied.

The hybrid windings employed in Ref. [77] adopted PCB windings, as shown in Figure 24. In Refs. [79, 80], a miniature axial flux motor with a prototype diameter of 17 mm was proposed, as shown in Figure 25. The motor employed rhomboidal PCB windings to obtain a back EMF similar to a sinusoid and shortened the length of the winding ends to reduce copper loss. In Ref. [81], non-overlapping concentric PCB windings that were simple in structure and highly reliable, could be flexibly modified, and easily achieved uniform distribution were adopted to replace the traditional coil winding filled with epoxy to achieve better manufacturability. The winding shape was changed into a hexagonal asymmetric structure by inclining the conductors of the trapezoidal winding at a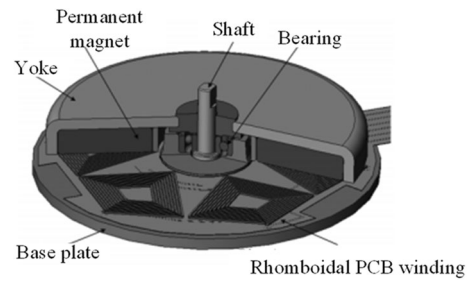n angle, as shown in Figure 26, to obtain a motor with a less copper loss than that in a trapezoidal PCB winding. For further optimization, the radial length of the coil was increased by 50% to couple the rotor flux linkage, which ultimately increased the ratio of torque-to-copper loss by 21%. In Ref. [82], a multilayer PCB was applied to a dual-stator–triple-rotor DCPMSM, and the eddy-current losses in the winding were reduced by connecting eight PCB boards in parallel.

Regarding the issue of back-EMF distortion in hexagonal or trapezoidal PCB stator windings, a non-overlapping wave-type distributed winding was proposed in Ref. [83] to minimize harmonics in the back EMF, thereby reducing the high-frequency rotor core loss. Figure 27 shows the structure of the new winding. Meanwhile, to reduce the copper loss resulting from the small-track cross-sectional area of the PCB windings, the number of layers on the PCB was optimized to 12. Additionally, the Halbach array was used to increase the air-gap magnetic flux density and achieve a motor efficiency of 96% at 30000 r/min.

4.3 Material Optimization

DCPMSMs have been studied to look for alternative materials for windings and rotors with excellent performance. Alternative conductor materials for windings have been studied, such as aluminum or carbon nanotubes (CNTs), to improve their torque-to-mass ratios [84]. Figure 28 shows a comparison of the winding
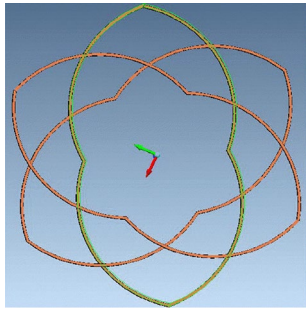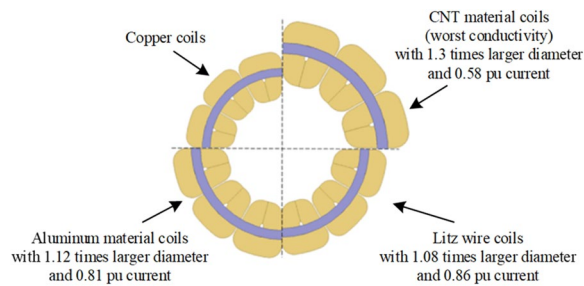
Figure 27 Winding structure proposed in Ref. [83]

Figure 28 Comparison of the winding diameters of various materials under the same torque-loss ratio
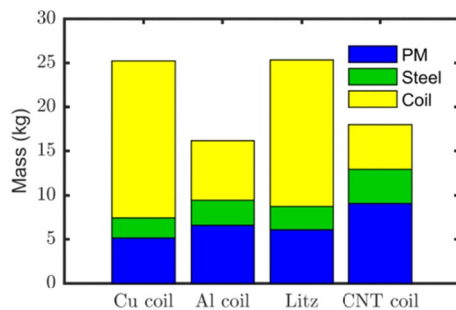

Figure 29 Total weight and component proportions of motors fabricated using copper, Litz wire, aluminum, and CNT coils

diameters of various materials under the same torque-loss ratio. CNTs exhibit the smallest mass density; therefore, a CNT motor is lighter. Figure 29 shows the total weight and proportion of each motor component composed of copper, aluminum, Litz wire, and CNT coils. The CNT-based motor exhibits the lowest coil mass ratio.

Figure 30 shows the power per unit mass and volume of a coreless AFPMSM fabricated using various coil materials at various speeds. The CNT-based motor demonstrates a better power per unit mass than the copper-based motor at high speeds. Therefore, a CNT coil is more suitable for applications with higher quality requirements. The final experimental results showed that aluminum had the advantage of being lightweight and low cost and that CNTs were lighter and exhibited no skin effect to reduce losses.

5 Minimization of Cogging Torque

Torque-ripple suppression has always been a major topic in AFPMSM research, particularly in low-speed applications, and the torque ripple generated by a motor and inverter may cause serious problems [85, 86]. Torque ripple affects torque quality, system performance, and vibration noise. Cogging torque is one of the main torque-quality problems addressed by motor design. Cogging torque is the torque ripple caused by the interaction between the permanent-magnetic field and variable-stator reluctance generated by the stator slot [87]. This is owing to the uneven distribution of the air-gap magnetic flux. To obtain better torque and speed performance, cogging torque must be minimized.

Cogging torque is mainly generated because of motor-design defects, and the stator current does not contribute to the generation of the cogging torque. Therefore, cogging torque minimization is mainly used to optimize the motor design, including magnet skew, pole-arc, dummy slot, and ratio of rotor-pole to stator-slot numbers [88, 89].
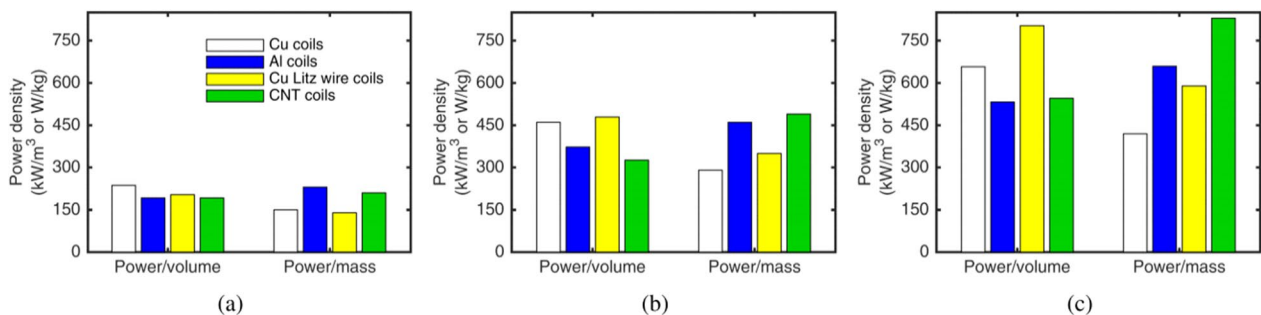

Figure 30 Power per unit mass and volume of coreless AFPMSMs fabricated using various coil materials at **a** 3600 r/min, **b** 7000 r/min, and **c** 10000 r/min

M. Aydin has made a significant contribution to the study of cogging-torque minimization. In 2003, he investigated the best magnetic pole-arc ratio in the range 0.333–1.000 to minimize cogging torque and compared the stator-side and rotor-side cogging-torque minimization techniques for a 24-slot 8-pole single-stator–dual-rotor motor. He analyzed the effects of optimizing the ratio of rotor-pole to stator-slot numbers, number of dummy slots in the stator teeth, magnet pole-arc, stator slot skew, rotor magnet skew, magnet or pole displacement, and variable magnet pole arc. Figure 31 shows several skewing techniques for AFPMSMs. From a cost point of view, stator-side cogging-torque minimization is not ideal. A comparative analysis [90] indicated that slot skew, magnet skew, and permanent-magnet shape improvement were the most commonly used and effective cogging-torque minimization methods. Therefore, in Refs. [87, 91], FEA was used to study the AFPMSM magnet skew technology for various magnetic pole-arc ratios and shapes. The final experimental results are shown in Figure 32. When the magnetic pole-arc ratio was 0.778, the peak cogging torque of the fan-shaped magnets was 37.5% and 62.5% higher than those of parallel-sided and circular magnets, respectively, and the triangular skew magnets were the most cost-effective and effective.

In Ref. [92], the effect of magnet asymmetry on minimizing the cogging torque of an AFPMSM with an integer pole/slot/phase was studied and a motor with shifted and skewed magnets was designed. Furthermore, the effects of magnet skewing and shifting on reducing cogging torque were experimentally verified. In Ref. [93],
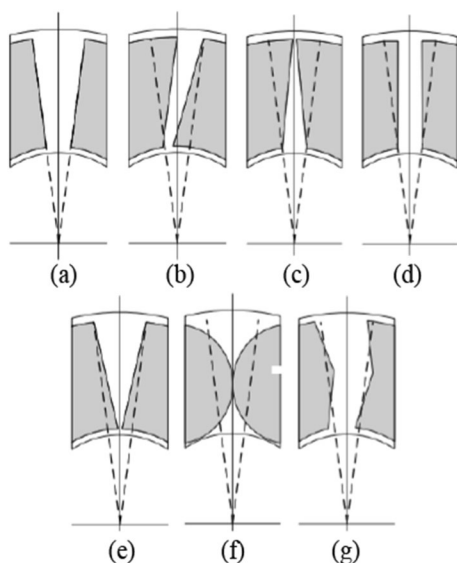

Figure 32 Peak-to-peak cogging torque comparison diagram

the asymmetrical bidirectional magnet skewing (ABMS) technique was applied to an AFPMSM. By comparing the three types of ABMS (ACAC, ACCA, and AACC) with various cross positions and skew angles, the effect of ABMS on minimizing the cogging torque was verified, and the applicable range of each structure was analyzed. Figure 33 shows the three ABMS layout methods. Tiegna et al. proposed a double-magnet skew technology and compared it with traditional and fan-shaped magnet-skew technologies [94]. The effect of double-magnet skew on cogging-torque minimization was verified experimentally, and the double-magnet skew technology was found to have a lesser effect on motor performance.

To better understand the principle of cogging torque and analyze the effect of the frequency and amplitude of cogging torque, an intuitive and accurate cogging-torque model must be developed. Generally, 3D-FEA is used for such an analysis; however, this method is limited in the discussion of optimal torque characteristics and is time consuming. Therefore, an analytical torque-calculation model has been proposed based on magnetic field analysis by employing the Maxwell tensor theory to derive and calculate the analytical model of cogging torque [95, 97]. Zuo et al. further used the radial pole-arc coefficient changing method, which employs various pole-arc coefficients of permanent magnets in the radial direction [97]. Thus, torque ripples of the opposite phase were

Figure 31 AFPMSM skewing techniques: **a** Unskewed, **b** Conventional, **c** Triangular, **d** Parallel-sided, **e** Trapezoidal, **f** Circular, and **g** Dual skewed
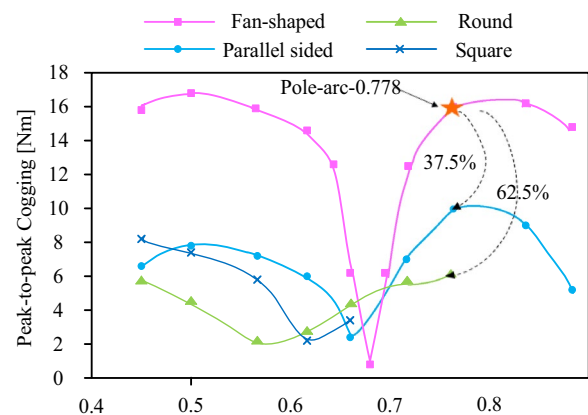

Figure 33 ABMS AACC, ACCA, and ACAC layouts

generated at various radii, and the cogging torque was effectively reduced; however, the obtained motor output performance was slightly lower.

To minimize the cogging torque via motor design, the parameter optimization method has been employed in motor design. In Ref. [98], an improved climb method was proposed using a multi-contour strategy to quickly determine the optimal motor parameters for cogging-torque minimization in a multidimensional optimization problem. Xu et al. established a response-surface model and combined it with a genetic algorithm to determine the optimal combination of the stator shoe-width ratio, magnet skew angle, and stator-shoe shift angle to minimize the cogging torque [59]. Sun et al. used the same parameter optimization method as Ref. [92], but the parameters were optimized for the magnet skewing angle, position angle, magnet skewing mode, magnetic pole-arc ratio, and structure of the reluctance rotor [89].

6 Control Strategy Optimization

To further optimize motor design and materials, improvements in motor control strategies have been investigated. To reduce torque ripple, the PSO algorithm has been used to optimize the parameters of the proportional integral (PI) controller. Experiments have shown that this method can effectively reduce the torque ripple and improve the stability of the control system. Neural networks and fuzzy control strategies have also been introduced to reduce torque fluctuations. For the torque-distribution optimization of multi-disc AFPMSMs, simulated annealing and genetic algorithms have been employed to design the torque distribution of motors, reduce system losses, and widen the high-efficiency interval.

6.1 Efficiency Optimization Strategy

Disc motors have emerged as alternatives to RFPMSMs for drive motor applications requiring high-power density and operating efficiencies such as electric vehicles, wind-power generation, and ship drives [11]. To further optimize operational efficiency, efficiency-optimization control strategies must be investigated. At present, there are two main efficiency-optimization control strategies for AFPMSMs: torque distribution and winding switching.

Efficiency-optimization control strategies are mainly aimed at systems driven by AFIR or multi-disc motors. Among them, the dual-stator–single-rotor motor exhibits a small moment of inertia, compact structure, and small mass [99]. The two stators are symmetrically placed on both sides of the rotor such that the middle rotor receives two magnetic forces that offset each other. The stator windings exhibit good heat-dissipation

performance, more stable structures, and less mechanical losses. Therefore, AFIR motors are suitable for applications requiring high efficiencies and torque densities [100]. Additionally, multi-disc motors such as three-stator–double-rotor disc motors meet the requirements for large torque outputs via coupling while ensuring a higher load rate under the same load.

6.1.1 Torque Distribution

The goal of the torque-distribution-efficiency optimization strategies is to obtain a high operating efficiency under the same speed and torque settings. Based on the efficiency map, torque distribution is carried out on each disc of the disc motor to achieve real-time switching of the motor working state, widen the high-efficiency range of the motor operation, and improve the global efficiency of the system [33, 34, 101, 102].

Using this control strategy, the two stator windings in a dual-stator motor are separately controlled by two sets of inverters, and the double-stator drives the rotor. Therefore, structurally, the two motors can be regarded as coaxially driven. Thus, the system topology of the efficiency-optimization control strategy can be obtained, as shown in Figure 34 [33]. The cooperative optimization controller receives control signals and torque data from the vehicle controller through the external Controller Area Network (CAN), determines the working state and torque of multiple motor modules according to the preset control strategy, and transmits it to multiple motor controllers through the internal CAN unit. Additionally, the collaborative optimization controller receives the motor status information fed back from the motor controller simultaneously and integrates the status information of multiple motor modules into one motor status information, where the current is the sum of the current of multiple motor modules along with the maximum voltage value.
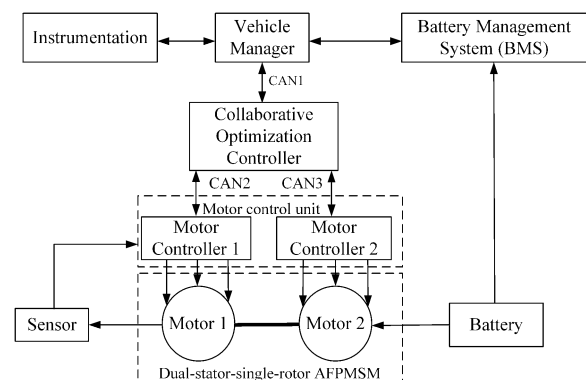

Figure 34 Efficiency optimization control strategy system topology diagram

In Ref. [34], an AFIR motor was used for efficiency optimization control. In this study, the motor drive system was divided into two operation modes: single and double windings. The efficiency map of the two modes was analyzed, and high-efficiency operating modes at different torques and speeds were selected to obtain the optimal operation efficiency diagram of a dual-stator motor. Simultaneously, the torque-coordinated control strategy was combined to reduce the torque mutation caused by mode switching, thereby reducing the impact of current on the inverter.

In Ref. [102], PSO was used for torque distribution optimization to improve the system efficiency and was applied to energy feedback to further improve the system operational efficiency. Moreover, to overcome the nonlinear interference of the system and improve the accuracy of the identification of the counter electromotive force, an adaptive robust control method was used in the current controller.

In Ref. [101], a three-stator-dual-rotor motor was used as the object, and a BP neural network was used to optimize the torque distribution mode with optimal efficiency to improve the operating range by approximately 15% under two-ton and no-load conditions. Simultaneously, a current controller based on deadbeat current prediction control was designed to improve the dynamic and steady-state response capabilities of the motor current loop and optimize the torque tracking characteristics.

In Ref. [103], a three-module AFPMSM was studied, and each module adopted a DSSR-AFPMSM structure. A genetic algorithm was used to allocate torque to two stator units within the same module, and the current optimal torque allocation coefficient was calculated at each torque speed point to achieve a cooperative optimization of efficiency.

In Ref. [104], based on an asymmetric DSSR-AFPMSM control system, an optimal torque allocation strategy based on the simulated annealing algorithm was proposed to broaden the high-efficiency interval of an AFPMSM under comprehensive operating conditions to obtain optimal torque allocation for system efficiency. The effectiveness of the allocation strategy was verified via simulations and experiments.

6.1.2 Winding Switching

The winding-switching method was originally used for asynchronous motors driven by a single inverter. The windings can be switched between parallel and series windings to obtain a large starting torque [105]. Xu et al. applied the winding switching control strategy to a PMSM for electric vehicles. By designing a single-stator PMSM with two sets of identical armature windings, winding switching control was carried out in series and parallel to improve the low-speed climbing and starting acceleration abilities of an electric vehicle and improve the operating efficiency of the system. As shown in Figure 35, the winding connection under the series operation condition was switched with the turning speed as the working condition boundary. The two sets of windings of the motor were in series when the vehicle started accelerating or climbing at a low speed. When the speed accelerated to the turning speed of the motor winding in a series operation, the winding switched to a parallel operation to continue the acceleration [106]. In 2014, Wang proposed a strategy to switch between series and parallel windings and single windings of dual-stator motors to achieve low-speed high-torque and high-speed low-torque operations and improve system operation efficiency [107].

The winding switching method for a dual-stator motor was applied to an AFPMSM controlled independently by multiple inverters to increase the high-efficiency range of motor operation; a redundant power supply was provided using multiple inverters. In Ref. [108], the winding switching control of a dual-stator disc motor was implemented. To operate single, series, and parallel windings, each phase winding was controlled by three switches as shown in Figure 36. The switch control states are shown in Table 4, where "0" denotes switch off and "1" denotes switch on. The winding-switching boundary was obtained by analyzing and comparing the optimal efficiencies of the winding switching method in different operating areas. Finally, the stator windings were operated in series at low speeds to improve the torque output capability. When the motor was running at a high speed, the stator windings were operated in parallel to expand the weak magnetic range, thereby greatly improving the power density, torque quality, and efficiency of the system. Additionally, a phase-shifting method based on an inverter PWM carrier effectively reduced the integrated torque ripple to address the problem of a large torque ripple in the parallel winding operation.

In summary, the two efficiency optimization control strategies were based on the efficiency map chart
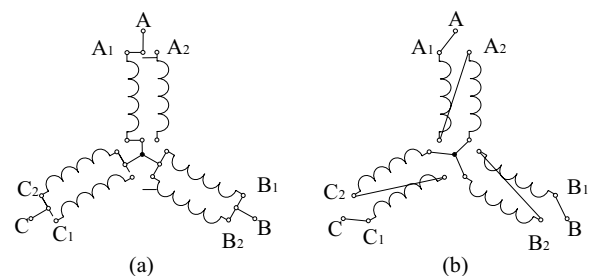

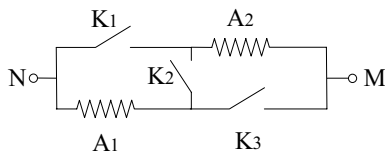**Figure 35** Winding connection methods: **a** Parallel and **b** Series

Figure 36 Distribution diagram of winding changeover switches

Table 4 On-off state of change-over switch

Serial number	Working winding	K_1	K_2	K_3
Mode1	A_1	0	0	1
Mode2	A_2	1	0	0
Mode3	$A_1 A_2$ in series	0	1	0
Mode4	$A_1 A_2$ in parallel	1	0	1

and expanded the high-efficiency operating range of an AFPMSM by switching the operating modes. However, both methods have advantages and disadvantages. The winding switching strategy requires nine switching devices to realize winding switching; therefore, the control is complex, and the possibility of failure is increased. The switching mode of the torque distribution strategy does not involve switching devices on and off and is obtained by changing the given torque. However, the torque-distribution strategy has a current mutation when the working condition is switched and may affect the inverter, whereas there is no effect on current during winding switching. Both methods use offline data as the basis for determining the working boundary, while the motor operating efficiency varies considerably according to the running condition; therefore, the method for determining the online working condition needs to be studied further.

6.2 Electromagnetic Torque-ripple Minimization Strategies for DCPMSMs

The elimination of a DCPMSM core causes the inductance of the stator winding to be too small and causes electromagnetic torque fluctuation [109, 110]. Because the DCPMSM has no core, the inductance of the stator winding is very small and leads to a fast change in the stator current. Owing to the limitation of the inverter switching frequency, the current in the stator winding cannot be continuous and results in electromagnetic torque fluctuations caused by the current in the motor without a tooth groove. Several studies have been conducted to solve this problem. Two control methods were proposed by Guang at Tianjin University. In the first method, the carrier frequency in the PWM control mode was improved, and the corresponding

high-frequency inverter was configured to alleviate electromagnetic torque fluctuation. However, the inductance of the motor was too small, and the current of the motor still contained a large number of high harmonics that made the speed unstable. Moreover, owing to the limitations of Insulated Gate Bipolar Transistor (IGBT) technology, the frequency improvement was not obvious. The second method is the brushless DC mode control method based on a buck chopper circuit that controls a DCPMSM by controlling the brushless DC motor to reduce torque ripple.

In Refs. [109, 111], based on torque control, a current-source chopper circuit was added at the front end of the inverter bridge. The circuit is shown in Figure 37. The inductance current on the DC bus was adjusted by the PWM control of the switch tube on the bus to change the current in the stator winding of the motor in real time and achieve torque control. At the same time, the relationship between the electromagnetic torque and reverse electromotive force, rotor angle, and current were used to estimate the instantaneous torque, and a closed-loop torque control based on the current vector was realized to effectively reduce torque ripple.

In Ref. [110], by increasing the switching frequency of the drive circuit and given the insufficient voltage stress of the high-switching-frequency MOSFET inverter, a three-level midpoint-clamped inverter was proposed as shown in Figure 38. A modified finite control set–model predictive control algorithm was used to predict the expected voltage vector and neutral voltage deviation in the next control period to realize midpoint voltage balance and improve operational speed.

In Ref. [112], a multilevel cascaded H-bridge (MLCHB) circuit was applied to a DCPMSM control system consisting of several H-bridges in series. The circuit is shown in Figure 39. This structure eliminated the current ripple by combining the carrier shifts of each H-bridge. When the MLCHB is used in electric vehicles, its charge balance technology can be used to
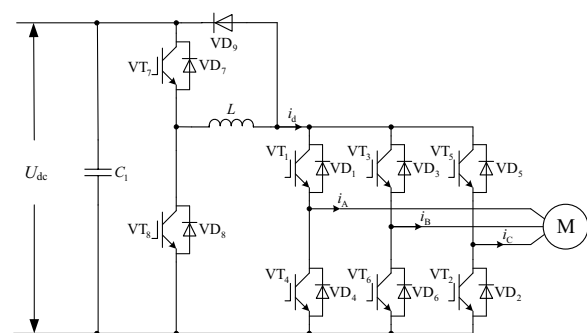

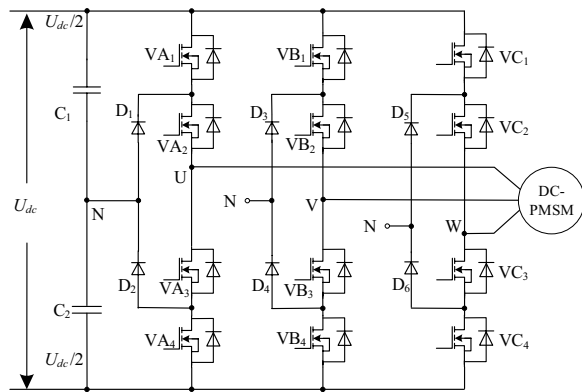**Figure 37** Current-source chopper circuit

Figure 38 Three-level midpoint-clamped inverter circuit

reduce the battery life reduction caused by unbalanced charge and discharge rates.

Improvements in control strategies for reducing torque ripple have gathered significant attention. Among them, direct torque control, model predictive control, fuzzy control, neural networks, and PSO are often applied.

Refs. [113, 114] used PSO to optimize a PI controller. In Ref.[113], a new control scheme for a motor drive system was proposed, and the PSO algorithm was used to optimize the parameters of the PI controller and improve the robustness of the control system. The experimental results showed that the proposed control strategy maximized the output torque and speed range of the drive system, and the PSO–PI controller reduced the torque ripple and improved the stability of the control system. In Ref. [114], a sensorless vector control strategy based on a higher-order sliding-mode observer (SMO) with a super-twisting algorithm was proposed. The general solution and multi-objective optimization characteristics of the PSO algorithm effectively tuned the PI coefficient to overcome the limitations of the traditional setting. Therefore, PSO was used to improve the gain of the PI controller to minimize the speed and torque fluctuations caused by the traditional PI parameter setting. In Ref. [115], an intelligent controller was designed for an AFPMSM. The controller was implemented as a neuro–fuzzy intelligent control system to eliminate the need for a bulky gearbox, and its feasibility was verified by manual measurements.

6.3 Synchronous Strategy of Contra-Rotating Rotors

A traditional AFPMSM rotor was synchronized with a magnetic field to ensure the stability of motor operation. For a dual-rotor motor, however, a CRPMSM has only one electrical end and two mechanical ends. When the load torque on the two rotors is unbalanced, it is difficult to satisfy the torque balance condition and leads to
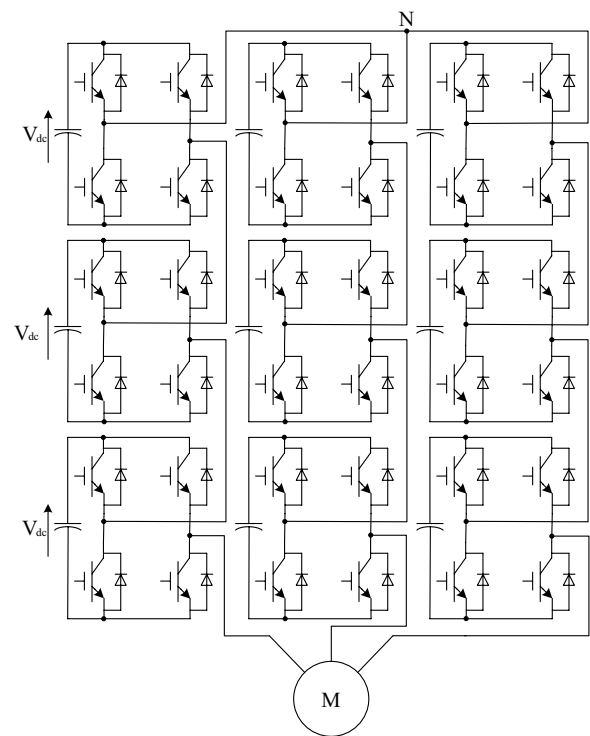

Figure 39 Multilevel cascaded H-bridge circuit

the rotor being out of step and without proper control. Therefore, ensuring the synchronous and stable operation of the two rotors is one of the main research prospects for CRPMSMs [116].

In Refs. [29, 117], control of a CRPMSM based on vector control was studied. The closed-loop control of a rotor with a large load was performed to realize the stability of the system with two permanent magnet rotors without loss of step under load imbalance or disturbance changes. The rotor-position detection method was adopted in Ref. [118]. After real-time detection and comparison of the two rotor positions, a dynamic master-slave control strategy was adopted to control the dual-rotor motor system to control and ensure the synchronous rotation of the two rotors under different load torque conditions. In Ref. [119], dynamic master-slave control and direct torque control were combined to reduce the dynamic system response time.

In Ref. [120], a dynamic sliding-mode control strategy that switched reference coordinate systems in real time was proposed to correct the operation instability of a CRPMSM when the load was unbalanced. The dynamic control of the two rotors was realized by comparing the torque angle in real time to switch the coordinate system required for control. To solve the problem of the dynamic control system being vulnerable to load disturbances, a non-singular fast terminal sliding-mode velocity

controller was constructed to improve the system robustness. However, two problems exist with the dynamic master-slave control method using a sliding-mode velocity controller: the robustness of the rotor is poor when the load mutation is large, and the torque ripple is large when the load is seriously unbalanced. Therefore, considering the problems in Ref. [120], Ref. [121] proposed a control strategy that combined dual-rotor direct torque control and load torque compensation. In this study, the load torques of the two rotors were obtained by the observer and feed-forward compensated to the direct torque control system.

7 Development Directions

At present, although AFPMSMs have many advantages over RFPMSMs, research on many aspects is still limited. Future research and development prospects are as follows:

(1) Multi physical field-coupling analysis

In the operation of an AFPMSM, multiple physical fields such as electromagnetic, temperature, and flow fields have mutual influence and equilibrium. Therefore, the coupling of each physical field must be considered in the motor design process, and the mutual influence should be analyzed. However, a perfect theoretical analysis system for multi-physical field coupling analysis is lacking, and research on the establishment and optimization of models considering multi-physical field coupling is also limited.

(2) Electromagnetic noise and vibration

Harmonics are an important cause of electromagnetic noise and vibration. At present, research on AFPMSM harmonic suppression mainly focuses on the spatial harmonics caused by the design defects motor bodies such as the tooth slot effect, magnetic circuit saturation effect, and winding distribution form that are suppressed through motor design optimization. However, the time-harmonic suppression caused by the nonlinear characteristics of inverters and the current detection error has rarely been studied in an AFPMSM control system. Research on motor vibration caused by multiple inverters in series and parallel and axial magnetic force is lacking.

(3) Multi-disc cooperative control technology

For AFPMSMs, inconsistent parameters between the stator or rotor, multi-disc drive and energy feedback braking, drive and field weakening control, and other multi-disc cooperative control technologies are subjects to be explored.

(4) Reliability research

Fault detection and fault-tolerant control are important technologies for improving the operational reliability of AFPMSMs. For multi-disc motors, faulty module detection, removal, and operation technologies are important manifestations of their structural advantages. Therefore, fault tolerance may be the focus of future studies.

8 Conclusions

With the demand for renewable energy generators and transport, AFPMSMs have attracted significant attention. Thus, with the deepening of research on AFPMSMs in related fields, their application scope becomes more extensive. In this review, the basic topological structures and classification of AFPMSMs, the design optimization methods of AFPMSMs with or without a core, the cogging torque minimization method, and the efficiency optimization strategy were reviewed. The basic structures, designs, and control methods of CRPMSMs and DCPMSMs were reviewed, and the development directions for AFPMSMs were summarized.

Author contributions
JZ: Supervision, Conceptualization of this study, Methodology. XL: Data curation, Writing an original draft, Writing review editing. SW: Conceptualization of this Methodology, Writing-review editing. LZ: Data curation, Validation. All authors read and approved the final manuscript.

Authors' information
Jianfei Zhao, born in 1977. He received the B.S. and M.S. degrees in mechatronic engineering from *Xi'an Jiaotong University, Xi'an, China*, in 2000 and 2003, respectively. He received his Ph.D. degree in electrical engineering from *Shanghai Jiao Tong University, Shanghai, China*, in 2012. From 2003 to 2006, he worked as a RD Engineer and Project Manager in *RD Center of Mywaylabs Co. Ltd., Japan*. Now, he is working as an associate professor with *School of Mechatronic Engineering and Automation*, *Shanghai University, China*. He is the author of more than 50 academic papers. His research interests include power electronics and electronic vehicles.
Dr. Zhao was a recipient of the Science and Technology Progress Award of the Ministry of Education of China in 2009 and 2012, the Science and Technology Progress Award of China Electrotechnical Society in 2009 and 2010.
Xiaoying Liu, born in 1998. She received the B.S. degree in electrical engineering and automation from *Shanghai University, China*, in 2020. She is pursuing the M.S. degree in electrical engineering, *Shanghai University, China*. Her research interests include electric vehicle drive control and new energy generation.
Shuang Wang, born in 1977. He received the B.S., M.S., and Ph.D. degrees in electrical engineering from the *Harbin Institute of Technology, China*, in 2000, 2005, and 2009, respectively. Since 2010, he has been with *School of Mechatronic Engineering and Automation*, *Shanghai University, China*, where he is currently an Assistant Professor. His current research interests include intelligent control theory and its application to new energy vehicles, power electronics, and servo control systems.
Lixiao Zheng, born in 1997. She received the B.S. degree in electrical engineering and automation from *Shanghai University, China*, in 2019. She is pursuing the M.S. degree in electrical engineering, *Shanghai University, China*. Her research interests include electric vehicle drive control and new energy generation.

References

[1]   P Campbell. Principles of a permanent-magnet axial-field DC machine. *Proceedings of the Institution of Electrical Engineers*, 1975, 121(12): 1489–1494.

[2]   P Campbell. The magnetic circuit of an axial field D.C. electrical machine. *IEEE Transactions on Magnetics*, 1975, 11(5): 1541–1543.

[3]   P Campbell, D J Rosenberg, D P Stanton. The computer design and optimization of axial-field permanent magnet motors. *IEEE Transactions on Power Apparatus and Systems*, 1981, PAS-100(4): 1490–1497.

[4]   Shuang Wang, Jianfei Zhao, Tingzhang Liu, et al. Adaptive robust control system for axial flux permanent magnet synchronous motor of electric medium bus based on torque optimal distribution method. *Energies*, 2019, 12: 4681.

[5]   G Rodrigues Bruzinga, A J S Filho, A Pelizari. Analysis and design of 3 kW axial flux permanent magnet synchronous motor for electric car. *IEEE Latin America Transactions*, 2022, 20(5): 855–863.

[6]   N Anitha, R Bharanikumar. Design and analysis of axial flux permanent magnet machine for wind power applications. *2019 International Conference on Power Electronics Applications and Technology in Present Energy Scenario (PETPES)*, 2019: 1–4.

[7]   P Ojaghlu, A Vahedi. Specification and design of ring winding axial flux motor for rim-driven thruster of ship electric propulsion. *IEEE Transactions on Vehicular Technology*, 2019, 68(2): 1318–1326.

[8]   D A Gonzalez, J A Tapia, A Letelier Bettancourt. Design consideration to reduce cogging torque in axial flux permanent-magnet machines. *IEEE Transactions on Magnetics*, 2007, 43(8): 3435–3440.

[9]   C Hwang, P Li, F C Chuang, et al. Optimization for reduction of torque ripple in an axial flux permanent magnet machine. *IEEE Transactions on Magnetics*, 2009, 45(3): 1760–1763.

[10] Y Lu, J Li, R Qu, et al. Electromagnetic force and vibration study on axial flux permanent magnet synchronous machines with dual three-phase windings. *IEEE Transactions on Industrial Electronics*, 2020, 67(1): 115–125.

[11] F Giulii Capponi, G De Donato, F Caricchi. Recent advances in axial-flux permanent-magnet machine technology. *IEEE Transactions on Industry Applications*, 2012, 48(6): 2190–2205.

[12] C C Chan. Axial-field electrical machines - design and applications. *IEEE Transactions on Energy Conversion*, 1987, EC-2(2): 294–300.

[13] N Chaker, I Salah, S Tounsi, et al. Design of axial-flux motor for traction application. *Journal of Electromagnetic Analysis Applications*, 2009, 1(2): 73–84.

[14] M Eker, M Akar, C Emeksiz, et al. Rotor design for line start AFPMSM. *IET Electric Power Applications*, 2019, 13(9):1273–1279.

[15] F Caricchi, F Crescimbini, O Honorati. Low-cost compact permanent magnet machine for adjustable-speed pump application. *IEEE Transactions on Industry Applications*, 1998, 34(1): 109–116.

[16] Y Huang, T Zhou, J Dong, et al. An overview on developments and researches of axial flux permanent magnet machines. *Proceedings of the Chinese Society of Electrical Engineering*, 2015, 35(1): 192–205. (in Chinese)

[17] J F Gieras, R J Wang, M J Kamper. *Axial flux permanent magnet brushless machines*. Springer Netherlands, 2004.

[18] M Aydin, S Huang, T Lipo. Axial flux permanent magnet disc machines: A review. *Conf. Record of SPEEDAM*, 2004, 1: 61–71.

[19] Z C Hao. *Study on electromagnetic performance and loss characteristics of axial-flux permanent magnet synchronous motor without core*. Harbin: Harbin Institute of Technology, 2020. (in Chinese)

[20] Wei Lu. *Electromagnetic field analysis of slot-free permanent magnet synchronous motor with axial magnetic field*. Wuhan: Huazhong University of Science and Technology, 2007. (in Chinese)

[21] Â P Ferreira, A F Costa. Thermal analysis of an axial flux permanent magnet machine. *2012th International Conference on Electrical Machines*, 2012: 1482–1487.

[22] M Drancă, M Chirca, Ş Breban, et al. Thermal and demagnetization analysis of an axial-flux permanent magnet synchronous machine. *2020 International Conference and Exposition on Electrical And Power Engineering (EPE)*, 2020: 200–204.

[23] H Vansompel, A Rasekh, A Hemeida, et al. Coupled electromagnetic and thermal analysis of an axial flux PM machine. *IEEE Transactions on Magnetics*, 2015, 51(11): 1–4.

[24] W Le, M Lin, L Jia, et al. Design of a novel stator water-cooling system for yokeless and segmented armature axial flux machine. *2021 IEEE 4th Student Conference on Electric Machines and Systems (SCEMS)*, 2021: 1–4.

[25] Y Bi, F Chai, L Chen. The study of cooling enhancement in axial flux permanent magnet motors for electric vehicles. *IEEE Transactions on Industry Applications*, 2021, 57(5): 4831–4839.

[26] F Marcolini, G De Donato, F G Capponi, et al. Direct oil cooling of end-windings in torus-type axial-flux permanent-magnet machines. *IEEE Transactions on Industry Applications*, 2019, 57(3): 2378–2386.

[27] E Spooner, B Chalmers. 'TORUS': a slotless, toroidal-stator, permanent-magnet generator. *Electric Power Applications, IEE Proceedings B*, 1992, 139(6): 497–506.

[28] F Caricchi, B J Chalmers, F Crescimbini, et al. Advances in the design of torus machines. *1998 International Conference on Power Electronic Drives and Energy Systems for Industrial Growth*, 1998, 2: 516–522.

[29] S Cheng, D Luo, S Huang, et al. Control strategy for permanent magnet synchronous motor with contra-rotating rotors under unbalanced loads condition. *IET Electric Power Applications*, 2015, 9(1): 71–79.

[30] F Caricchi, F Crescimbini, E Santini. Basic principle and design criteria of axial-flux PM machines having counterrotating rotors. *IEEE Transactions on Industry Applications*, 1995, 31(5): 1062–1068.

[31] S Huang, S Cheng, D Luo, et al. Design and characteristic analysis of an axial-flux permanent magnet synchronous motor with contra-rotating rotors. *Transactions of China Electrotechnical Society*, 2017, 32(12): 72–80. (in Chinese)

[32] Q Chen, D Liang, Y Liu, et al. Design and multi-object optimisation of axial flux interior PMSM for EV and HEV applications. *The Journal of Engineering*, 2017, 5: 2215–2220.

[33] M H, J Zhao, T Liu. Cooperative optimization and fault-tolerant control method of multi-disk permanent magnet synchronous motor for electric vehicles. *Proceedings of the CSEE*, 2019, 39(2): 386–394, 636. (in Chinese)

[34] J Zhao, M Hua, T Liu. Research on a sliding mode vector control system based on collaborative optimization of an axial flux permanent magnet synchronous motor for an electric vehicle. *Energies*, 2018, 11(11): 1.

[35] S Huang, Jian Luo, F Leonardi, et al. A general approach to sizing and power density equations for comparison of electrical machines. *IAS '96. Conference Record of the 1996 IEEE Industry Applications Conference Thirty-First IAS Annual Meeting*, 1996, 2: 836–842.

[36] A Parviainen, M Niemela, J Pyrhonen, et al. Performance comparison between low-speed axial-flux and radial-flux permanent magnet machines including mechanical constraints. *IEEE International Conference on Electric Machines and Drives*, 2005: 1695–1702.

[37] Surong Huang, Jian Luo, F Leonardi, et al. A comparison of power density for axial flux machines based on general purpose sizing equations. *IEEE Transactions on Energy Conversion*, 1999, 14(2): 185–192.

[38] M Khatab, Z Zhu, H Li, et al. Comparative study of novel axial flux magnetically geared and conventional axial flux permanent magnet machines. *China Electrotechnical Society Transactions on Electrical Machines and Systems*, 2019, 2(1): 392–398.

[39] B Scheerlinck, H De Gersem, P Sergeant. 3-D eddy current and fringing-flux distribution in an axial-flux permanent-magnet synchronous machine with stator in laminated iron or SMC. *IEEE Transactions on Magnetics*, 2015, 51(11): 1–4.

[40] A Daghigh, H Javadi, H Torkaman. Design optimization of direct-coupled ironless axial flux permanent magnet synchronous wind

Zhao et al. Chinese Journal of Mechanical Engineering　　　(2023) 36:45

Page 20 of 21

generator with low cost and high annual energy yield. *IEEE Transactions on Magnetics*, 2016, 52(9): 1–11.

[41] G Zhao, J Zhao, L Yang. An improved equivalent magnetic circuit model of coreless axial flux permanent magnet synchronous machine. *2017 IEEE International Magnetics Conference (INTERMAG)*, 2017: 1.

[42] J Choi, S Lee, K Ko, et al. Improved analytical model for electromagnetic analysis of axial flux machines with double-sided permanent magnet rotor and coreless stator windings. *IEEE Transactions on Magnetics*, 2011, 47(10): 2760-2763.

[43] X W, G Li, H Yu, et al. Magnet optimization of disc coreless permanent magnet synchronous motor based on Halbach. *Micromotors*, 2015, 48(2): 1-6, 43. (in Chinese)

[44] Changle Sun, Feng Wen, Wei Xiong, et al. Multi-objective comprehensive teaching algorithm for multi-objective optimisation design of permanent magnet synchronous motor. *IET Electric Power Applications*, 2020, 14(13): 2564-2576.

[45] G V Cvetkovski, L B Petkovska. Weight reduction of permanent magnet disc motor for electric vehicle using genetic algorithm optimal design procedure. *IEEE EUROCON 2009*, 2009, 881-888.

[46] Y Luo, D Tan. Lightweight design of an in-wheel motor using the hybrid optimization method. *Proceedings of the Institution of Mechanical Engineers, Part D: Journal of Automobile Engineering*, 2013, 227(12): 1590–1602.

[47] D Lim, Y Cho, J Ro, et al. Optimal design of an axial flux permanent magnet synchronous motor for the electric bicycle. *IEEE Transactions on Magnetics*, 2016, 52(3): 1–4.

[48] R Akinci, M Polat. Design and optimization with genetic algorithm of double rotor axial flux permanent magnet synchronous motor (torus type) for electrical vehicles. *2019 4th International Conference on Power Electronics and their Applications (ICPEA)*, 2019: 1–5.

[49] T J Woolmer, M D McCulloch. Analysis of the yokeless and segmented armature machine. *2007 IEEE International Electric Machines Drives Conference*, 2007, 1: 704–708.

[50] Q A S Syed, H Kurtovi¢, I Hahn. New single-phase flux switching axial flux permanent magnet motor. *IEEE Transactions on Magnetics*, 2017, 53(11): 1–5.

[51] M T Bin Tarek, Y Sozer. Design of a novel axial flux permanent magnet assisted synchronous reluctance motor. *2019 IEEE Energy Conversion Congress and Exposition (ECCE)*, 2019: 3004–3009.

[52] A Kampker, P Treichel, K Kreisköther, et al. Alternative fabrication strategies for the production of axial flux permanent magnet synchronous motors for enhanced performance characteristics. *2018 8th International Electric Drives Production Conference (EDPC)*, 2018: 1–7.

[53] N Fernando, F Hanin. Magnetic materials for electrical machine design and future research directions: A review. *2017 IEEE International Electric Machines and Drives Conference (IEMDC)*, 2017: 1–6.

[54] A Krings, J Soulard. Experimental characterization of magnetic materials for electrical machine applications. *2015 IEEE Workshop on Electrical Machines Design, Control and Diagnosis (WEMDCD)*, 2015: 85–89.

[55] N Fernando, G Vakil, P Arumugam, et al. Impact of soft magnetic material on design of high-speed permanent-magnet machines. *IEEE Transactions on Industrial Electronics*, 2017, 64(3): 2415–2423.

[56] Y G Guo, J G Zhu, P A Watterson, et al. Comparative study of 3D flux electrical machines with soft magnetic composite cores. *Conference Record of the 2002 IEEE Industry Applications Conference. 37th IAS Annual Meeting (Cat. No.02CH37344)*, 2022, 2: 1147–1154.

[57] C Kim, G Jang, J Kim, et al. Comparison of axial flux permanent magnet synchronous machines with electrical steel core and soft magnetic composite core. *IEEE Transactions on Magnetics*, 2017, 53(11): 1–4.

[58] N Ertugrul, R Hasegawa, W L Soong, et al. A novel tapered rotating electrical machine topology utilizing cut amorphous magnetic material. *IEEE Transactions on Magnetics*, 2015, 51(7): 1–6.

[59] L Xu, Y Xu, J Gong. Analysis and optimization of cogging torque in yokeless and segmented armature axial-flux permanent-magnet machine with soft magnetic composite core. *IEEE Transactions on Magnetics*, 2018, 54(11): 1–5.

[60] F Profumo, F J Eastham, A Tenconi, et al. "Plastic" electric motors: a viable solution for axial flux machines. *Industrial Electronics, Proceedings of the 2002 IEEE International Symposium*, 2022, 1(1): 1–10.

[61] J F Gieras, I A Gieras. Performance analysis of a coreless permanent magnet brushless motor. *Conference Record of the 2002 IEEE Industry Applications Conference. 37th IAS Annual Meeting (Cat. No.02CH37344)*, 2022, 4: 2477-2482.

[62] X Wang, J Chen, G Yu. The analysis and simulation of the armature magnetic field in coreless permanent magnet motor. *2009 International Conference on Electrical Machines and Systems*, 2009: 1–4.

[63] S Khan, S S H Bukhari, J Ro. Design and analysis of a 4-kW two-stack coreless axial flux permanent magnet synchronous machine for low-speed applications. *IEEE Access*, 2019, 7: 173 848–173 854.

[64] M Wu, Y Cao, Q Li. Optimal design of a coreless stator axial flux permanent-magnet motor based on particle swarm algorithm. *Proceedings of the 33rd Chinese Control Conference*, 2014: 8996–9001.

[65] F Pranji¢, P Virti£. Designing rotor disks of a coreless axial flux permanent magnet machines by using simplified fem and an approximation method. *IEEE Transactions on Energy Conversion*, 2020, 35(3): 1505–1512.

[66] W Le, M Lin, L Jia, et al. Multi-objective optimization of an air-cored axial flux permanent magnet synchronous machine with segmented PMS based on support vector machine and genetic algorithm. *2019 22nd International Conference on Electrical Machines and Systems (ICEMS)*, 2019: 1–4.

[67] M Aydin, M Gulec, Y Demir, et al. Design and validation of a 24-pole coreless axial flux permanent magnet motor for a solar powered vehicle. *2016 XXII International Conference on Electrical Machines (ICEM)*, 2016: 1493–1498.

[68] C Gu. Magnetic field analysis and optimization design of rotor-coreless DC permanent magnet disc motor. *Proceedings of the CSEE*, 1996, 16(2): 125–129. (in Chinese)

[69] Xiaoyuan Wang, Fang Zhao, Jingjuan Du, et al. The magnetic field simulation of multi-disc coreless magnet synchronous motor based on halbach array. *2005 International Conference on Electrical Machines and Systems*, 2005, 3: 2083–2086.

[70] X Wang, K Xiao. Analysis for magnetic field in the air gap of the wheel multi-disc coreless permanent magnet synchronous motor. *2009 International Conference on Electrical Machines and Systems*, 2009: 1–4.

[71] T S El-Hasan, P C K Luk. Magnet topology optimization to reduce harmonics in high-speed axial flux generators. *IEEE Transactions on Magnetics*, 2003, 39(5): 3340–3342.

[72] L del Ferraro, R Terrigi, F G Capponi. Coil and magnet shape optimization of an ironless afpm machine by means of 3D FEA. *2007 IEEE International Electric Machines Drives Conference*, 2007, 2: 927–931.

[73] M Aydin, M Gulec. A new coreless axial flux interior permanent magnet synchronous motor with sinusoidal rotor segments. *IEEE Transactions on Magnetics*, 2016, 52(7): 1–4.

[74] J F Gieras, I A Gieras. Performance analysis of a coreless permanent magnet brushless motor. *Conference Record of the 2002 IEEE Industry Applications Conference. 37th IAS Annual Meeting (Cat. No.02CH37344)*, 2002, 4: 2477–2482.

[75] Q L X Wang, S Wang. Analytical calculation of no-load air-gap magnetic field and back electromotive force in brushless dc motor. *Proceedings of the CSEE*, 2003, 23(3): 126–1307. (in Chinese)

[76] M J Kamper, R Wang, F G Rossouw. Analysis and performance of axial flux permanent-magnet machine with air-cored nonoverlapping concentrated stator windings. *IEEE Transactions on Industry Applications*, 2008, 44(5): 1495–1504.

[77] X Wang, Z Tian. Shape design of windings of disc-type electric machine with PCB stator. *Small Special Electrical Machines*, 2016, 44(2): 29–33.

[78] Y Zhang, N Liu, S Guo, et al. Analysis and design of ironless axial flux permanent magnet synchronous motor. *2018 10th International Conference on Intelligent Human-Machine Systems and Cybernetics (IHMSC)*, 2018, 2: 170–173.

[79] M Tsai, L Hsu. Design of a miniature axial-flux spindle motor with rhomboidal PCB winding. *IEEE Transactions on Magnetics*, 2006, 42(10): 3488–3490.

[80] Liang Yi Hsu, Chien Chin Huang, Mi Ching Tsai, et al. A no-coupling characteristic estimating method for a miniature axial-flux brushless motor. *2007 International Conference on Electrical Machines and Systems (ICEMS)*, 2007: 853–855.

[81] X Wang, C Li, F Lou. Geometry optimize of printed circuit board stator winding in coreless axial field permanent magnet motor. *2016 IEEE Vehicle Power and Propulsion Conference (VPPC)*, 2016: 1–6.

Zhao *et al. Chinese Journal of Mechanical Engineering*   (2023) 36:45

Page 21 of 21

[82]   X Wang, C Hu, M Zhao, et al. Design of multi-layer PCB coreless axial permanent magnet synchronous motor. *2019 22nd International Conference on Electrical Machines and Systems (ICEMS)*, 2019: 1–4.

[83]   N S, S P Nikam, S Singh, et al. High-speed coreless axial-flux permanent-magnet motor with printed circuit board winding. *IEEE Transactions on Industry Applications*, 2019, 55(2): 1954–1962.

[84]   V Rallabandi, N Taran, D M Ionel, et al. Coreless multidisc axial flux PM machine with carbon nanotube windings. *IEEE Transactions on Magnetics*, 2017, 53(6): 1–4.

[85]   M Aydin, Surong Huang, T A Lipo. Torque quality and comparison of internal and external rotor axial flux surface-magnet disc machines. *IEEE Transactions on Industrial Electronics*, 2006, 53(3): 822–830.

[86]   Y Qin, X Tang, T Jia, et al. Noise and vibration suppression in hybrid electric vehicles: State of the art and challenges. *Renewable and Sustainable Energy Reviews*, 2020, 124: 109782.

[87]   M Aydin, M Gulec. Reduction of cogging torque in double-rotor axial-flux permanent-magnet disk motors: A review of cost-effective magnet-skewing techniques with experimental verification. *IEEE Transactions on Industrial Electronics*, 2014, 61(9): 5025–5034.

[88]   M Aydin, Ronghai Qu, T A Lipo. Cogging torque minimization technique for multiple-rotor, axial-flux, surface-mounted-PM motors: alternating magnet pole-arcs in facing rotors. *38th IAS Annual Meeting on Conference Record of the Industry Applications Conference*, 2003, 1: 555–561.

[89]   S Sun, F Jiang, T Li, et al. Optimization of cogging torque in a hybrid axial and radial flux permanent magnet machine. *2019 22nd International Conference on Electrical Machines and Systems (ICEMS)*, 2019: 1–5.

[90]   M Aydin, Z Q Zhu, T A Lipo, et al. Minimization of cogging torque in axial-flux permanent-magnet machines: Design concepts. *IEEE Transactions on Magnetics*, 2007, 43(9): 3614–3622.

[91]   M Aydin. Magnet skew in cogging torque minimization of axial gap permanent magnet motors. *2008 18th International Conference on Electrical Machines*, 2008: 1–6.

[92]   M Gulec, M Aydin. Magnet asymmetry in reduction of cogging torque for integer slot axial flux permanent magnet motors. *Electric Power Applications, IET*, 2014, 8: 189–198.

[93]   H Xie, X Wei, Y Liu, et al. Research of asymmetrical bidirectional magnet skewing technique in modular multi-stage axial flux permanent magnet synchronous motor. *IEEE Transactions on Magnetics*, 2015, 51(3): 1–5.

[94]   L Jia, M Lin, W Le, et al. Dual-skew magnet for cogging torque minimization of axial flux PMSM with segmented stator. *IEEE Transactions on Magnetics*, 2020, 56(2): 1–6.

[95]   P Virtic, P Pisek, M Hadziselimovic, et al. Torque analysis of an axial flux permanent magnet synchronous machine by using analytical magnetic field calculation. *IEEE Transactions on Magnetics*, 2009, 45(3): 1036–1039.

[96]   H Tiegna, Y Amara, G Barakat. Study of cogging torque in axial flux permanent magnet machines using an analytical model. *IEEE Transactions on Magnetics*, 2014, 50(2): 845–848.

[97]   Shuguang Zuo, Shuanglong Wu, Xudong Wu, et al. Analytical model and optimization of torque of an axial flux permanent magnet synchronous motor. *Transactions of China Electrotechnical Society*, 2016, 31: 46–53.

[98]   D Woo, I Kim, D Lim, et al. Cogging torque optimization of axial flux permanent magnet motor. *IEEE Transactions on Magnetics*, 2013, 49(5): 2189–2192.

[99]   Chengtsung Liu, Kunchin Chuang. Mathematical modeling and field-oriented control of a disc-type surface-mounted permanent magnet motor. *2002 IEEE International Magnetics Conference (INTERMAG)*, Amsterdam, Netherlands, 2002.

[100] P R Upadhyay, K R Rajagopal, B P Singh. Design of a compact winding for an axial-flux permanent-magnet brushless DC motor used in an electric two-wheeler. *IEEE Transactions on Magnetics*, 2004, 40(4): 2026–2028.

[101] J Zhao, L Zheng, S Wang, et al. Research on deadbeat current prediction vector control system of axial flux permanent magnet synchronous motor for electric bus based on efficiency optimal torque distribution method. *IEEE Access*, 2019, 7: 128 384–128 393.

[102] J Zhao, Q Han, Y Dai, et al. Study on the electromagnetic design and analysis of axial flux permanent magnet synchronous motors for electric vehicles. *Energies*, 2019, 12(18): 3451.

[103] Jianfei Zhao, Qian Xiang, Shuang Wang. Efficiency optimization control method of modular AFPMSM with wide speed range for electric vehicle. *Proceedings of CSEE*, 2022, 1-10.(in Chinese)

[104] Jianfei Zhao, Yongqun Jiang, Deliang Wu. Drive control strategy of asymmetric double-disk permanent magnet synchronous motor for electric vehicle in full speed domain. *Proceedings of CSEE*, 2022: 1-11. (in Chinese)

[105] Hong Huang, Liuchen Chang. Electrical two-speed propulsion by motor winding switching and its control strategies for electric vehicles. *IEEE Transactions on Vehicular Technology*, 1999, 48(2): 607–618.

[106] Yanliang Xu, Jiaqun Xu, Wenbin Wan, et al. Development of permanent magnet synchronous motor used in electric vehicle. *ICEMS'2001. Proceedings of the Fifth International Conference on Electrical Machines and Systems (IEEE Cat. No.01EX501)*, 2001, 2: 884–887.

[107] Y Wang, Y Xu. Winding switching analysis of dual-stator permanent magnet brushless DC motors used in electric vehicles. *Transactions of China Electrotechnical Society*, 2014, 29: 98–103.

[108] Y Zhang, K Yang, H Xie, et al. Optimal efficiency control of modular pmsm on EVs based on ISO efficiency contours. *2014 17th International Conference on Electrical Machines and Systems (ICEMS)*, 2014: 2131–2135.

[109] X Wang, X Wang, T Fu, et al. Predictive instantaneous torque control for disc coreless permanent magnet synchronous motor with the current source chopper. *IEEE Transactions on Power Electronics*, 2015, 30(12): 7100–7112.

[110] X Wang, W Xu, Y Zhao, et al. Modified MPC algorithm for NPC inverter fed disc coreless permanent magnet synchronous motor. *IEEE Transactions on Applied Superconductivity*, 2016, 26(7): 1–5.

[111] Xiaoyuan Wang, Xiaoguang Wang, Tao Fu. Instantaneous torque control for disc coreless permanent magnetic synchronous motor drives based on the current vector. *Transactions of China Electrotechnical Society*, 2016, 31(16): 43-49.

[112] K W Sun, T J Summers, C E Coates. Ironless axial flux permanent magnet motor control with multilevel cascaded H-bridge converter for electric vehicle applications. *2016 IEEE 2nd Annual Southern Power Electronics Conference (SPEC)*, 2016: 1-6.

[113] J Zhao, M Lin, D Xu, et al. Vector control of a hybrid axial field flux-switching permanent magnet machine based on particle swarm optimization. *IEEE Transactions on Magnetics*, 2015, 51(11): 1-4.

[114] R Wilson, R Gandhi, A Kumar, et al. Performance analysis of twin-rotor axial flux permanent magnet synchronous motor for in-wheel electric vehicle applications with sensorless optimized vector control strategy. *2020 IEEE International Conference on Power Electronics, Drives and Energy Systems (PEDES)*, 2020: 1-6.

[115] S Nazlibilek, E Mohammed. Neuro-fuzzy controller for axial flux permanent magnet gearless generator. *2019 IEEE International Conference on Fuzzy Systems (FUZZ-IEEE)*, 2019: 1-6.

[116] S Cheng, S Huang. Independent torque control of two rotors of an axial-flux PMSM with contra-rotating rotors using a single inverter. *2014 IEEE Conference and Expo Transportation Electrification Asia-Pacific (ITEC Asia-Pacific)*, 2014, 1–5.

[117] Y Zhong, S Huang, D Luo, et al. Speed synchronism of permanent magnet synchronous motor with dual contra-rotating rotors under load variation. *IET Power Electronics*, 2017, 10(12): 1479-1486.

[118] Y Zhong, S Huang, D Luo, et al. Speed synchronism for contra-rotating permanent magnet synchronous motor system and its control strategy. *Diangong Jishu Xuebao/Transactions of China Electrotechnical Society*, 2018, 33: 1478–1487. (in Chinese)

[119] Yan Jiang, Zhong Huang, Shuangyin Cheng, et al. A direct torque control strategy of counter-rotating permanent magnet synchronous motors. *Transactions of China Electrotechnical Society*, 2015, 30: 101–107.

[120] Derong Luo, Ruizhi He, Shoudao Huang, et al. Dynamic sliding mode control for single stator dual rotor disc counter-rotating permanent magnet synchronous motor. *Transactions of China Electrotechnical Society*, 2019, 34(9): 1806–1814.

[121] Derong Luo, Xin Su, Ruizhi He, et al. Dual-rotor direct torque control strategy of disk-type contra-rotating permanent magnet synchronous motor under heave unbalanced load torque. *Transactions of China Electrotechnical Society*, 2019, 34(22): 4678–4686.